Tumbling Magnetic Microrobots for Biomedical Applications

Chenghao Bi[1], Elizabeth E. Niedert[2], Georges Adam[1], Elly Lambert[2],
Luis Solorio[3], Craig J. Goergen[3], and David J. Cappelleri[1]

***Abstract*— This paper presents a magnetic microrobot that demonstrates the ability to travel through wet conditions inside a murine colon. Under the influence of an external rotating magnetic field, it tumbles end-over-end to propel itself forward. The microrobot's real-time position can be accurately tracked using ultrasound imaging to help guide it to a desired target location. Diffusion tests were conducted and show that the microrobot releases a fluorescein payload over a two hour time period when it is applied as a coating. Cytotoxicity tests demonstrated that the microrobot's SU-8 body doped with magnetic NdFeB particles is also biocompatible with murine fibroblasts. The microrobot's capabilities make it promising for targeted drug delivery and other *in vivo* biomedical applications.**

I. INTRODUCTION

Recent advances in microfabrication techniques have resulted in a surge of growth in the variety and capabilities of microrobots for biomedical applications [1], [2]. At this scale, robots must be able to maintain functionality in spite of a very small footprint, maintain forward motion through low Reynolds number environments, and negotiate with the increased impact of forces that scale with area and distance [3], [4]. To this end, many innovative solutions have been devised to make functionality at the microscale possible, incorporating a variety of actuation methods that take advantage of acoustic, ultrasound, optical, thermal, chemical, or magnetic stimulus [5]. Due to their relatively small dimensions, approximately the size of a human cell, microrobots have unparalleled access to areas of the body that are difficult or impossible to reach using conventional macroscale tools. Their diminutive size makes them especially advantageous for minimally invasive operations and precise, localized treatment. These qualities could result in reduced patient trauma, a lower risk of side effects, and higher drug retention rates compared to traditional surgical techniques and passive drug diffusion. Critical applications such as targeted drug delivery, precision surgery, biosensing, and detoxification have already been demonstrated to be feasible in both *in vitro* and *in vivo* test cases. For example, Gao et al. introduced an acid-driven micromotor that presses a drug payload directly against the stomach walls of live mice [6]. Tetherless microgrippers have also been developed that respond to fluctuations in local temperature, acidity, or enzyme stimuli [7] and high-speed, ultrasound actuated microbullets have been shown to be capable of deep tissue penetration [8]. Functionalizing microrobots with different bioreceptors allows desired proteins and cells to bind to them and incorporating features such as nanosponges into their design allows microrobots to absorb and neutralize toxins within the body [9].

Of particular interest are colonoscopies, which are necessary to examine and diagnose colorectal cancer and inflammatory bowel disease. These two ailments affect millions worldwide and can cause fatigue, bloody diarrhea, weight loss, and abdominal pain [10]. Due to the invasiveness of the colonoscopy procedure, patients often experience extreme discomfort and reluctance to undergo further examination [11]. Additionally, colonoscopies themselves have the potential to exacerbate existing disease symptoms [12]. The use of ultra-thin colonoscopes has been shown to significantly improve tolerability in patients [13]. Non-invasive options such as bowel ultrasounds [14] and quantitative fecal immunochemical tests [15] also exist and can provide partial colon screening. Despite these options, no solution has fully eliminated the need for colonoscopies. The introduction of a microrobotic alternative, however, could lead to new non-invasive procedures that reduce patient discomfort and open new possibilities in disease diagnosis.

For microrobots aimed towards biomedical applications, magnetic actuation continues to be a widely used choice. It does not require a controlled, specialized environment to operate and external magnetic fields harmlessly penetrate living tissue. Helical magnetic microswimmers have already been shown to capture and deliver sperm cells for potential applications in treating infertility [16]. Rolling magnetic microrobots such as "RodBot" [17] are able to trap and manipulate objects using non-contact methods in fluid environments. Elastomeric, nonuniformly-aligned magnetic millibots have also been shown to be capable of a wide variety of locomotive gaits [18]. This paper will focus on a robust, rigid magnetic microrobot that moves by tumbling end-over-end to traverse through both wet and dry environments. Section II discusses the background and overview of the robot design, as well as the fabrication methods. Section III presents the experimental setup, results, and discussion of using these microrobots for biomedical applications. These experiments

This work was supported by NSF IIS Award #1358446 and NSF NRI Award #1637961. E.E.N. was supported by a Mark and Pamela Lamp Graduate Scholarship. L.S. and E.L. were supported by the National Cancer Institute (R0CA19829 to L.S.).

[1]C. Bi, G. Adam, and D. Cappelleri are with the School of Mechanical Engineering, Purdue University, West Lafayette, IN 47907, USA {bi10,adamg,dcappell}@purdue.edu

[2]E. Niedert and E. Lambert are with the Weldon School of Biomedical Engineering, Purdue University, West Lafayette, IN 47907, USA {eniedert,lamberte}@purdue.edu

[3]L. Solorio and C. Goergen are with the Weldon School of Biomedical Engineering and the Purdue Center for Cancer Research, Purdue University, West Lafayette, IN 47907, USA {lsolorio,cgoergen}@purdue.edu

include locomotion tests conducted inside murine colons and phantom tissue tubes, real-time ultrasound imaging, payload diffusion over time studies, and cytotoxicity tests of the robot's constituent material. Finally, several conclusions and a future outlook is provided in Section IV.

II. DESIGN OF MICROROBOT

A. Background

While the majority of microrobots for biomedical applications are intended to operate in liquid environments, there are numerous areas in the human body containing a combination of both liquid and dry environments, posing challenges for microrobot movement. These areas include pockets of air and mucous within the lungs and along the digestive tract. Many existing magnetic microrobot designs use external field gradients to move, but this form of actuation is not viable in dry environments. The pulling force induced from the field gradients is often not strong enough to overcome the high stiction forces, a combination of frictional and adhesive forces, between the microrobots and the surfaces they rest on. Other forms of magnetic actuation and locomotion are more practical for overcoming this increased stiction. Drawing inspiration from living organisms, these forms include crawling, rolling, walking, and jumping. Hu et al. demonstrated a magneto-elastic millirobot capable of many of these locomotive gaits [18], but the technology has yet to be miniaturized to the microscale. At this smaller scale, some solutions for magnetic locomotion through dry environments include stick-slip motion [19] and oscillating micro-swing hammers [20], but many of these methods include a point along the locomotive gait where the microrobot loses contact with the surface and the resulting motion becomes uncontrolled over rough terrain. This behavior makes it difficult for these robots to travel over the complex surfaces present throughout the body.

Jing et al. introduced a dumbbell-shaped microrobot that moves in a tumbling motion and maintains constant contact with the surface [21]. The robot is actuated by an external magnetic field that alternates between a vertical and horizontal alignment, inducing magnetic torque on the robot and causing it to rotate. By tumbling instead of sliding or slipping forward, the microrobot uses stiction to its advantage and grips onto the surface. The design was improved upon in [22], where the alternating field was replaced with a rotating field. This change allowed the robot's fabrication process to be simplified, where the entire magnetic body could be aligned uniformly while still moving in the same manner as before. The newer design was shown to be capable of moving predictably in dry environments over multiple complex terrains and climb inclines of up to 45°.

B. Microrobot Design

Fig. 1(a) illustrates the microrobot used in this paper, a solid 800 x 400 x 120 μm polymeric block that is doped with magnetic neodymium iron boron (NdFeB) microparticles. This doping process can generate hard magnets that can be magnetically aligned irrespective of geometry or particle orientation. Two circular cut-outs 200 μm in diameter allow the robot to store additional payload material in addition to any material coating the outer surface. The magnetic particles are aligned along the length of the robot by exposing them to a 9 T uniform magnetic field oriented in the same direction. Due to orientation differences between the microrobot's magnetic alignment and that of the external actuating field, seen in Fig. 1(b), a magnetic torque is induced on the robot:

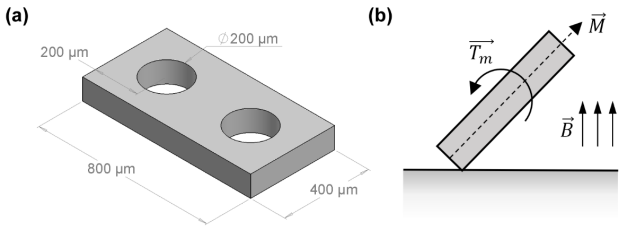

Fig. 1. (a) Dimensions of tumbling magnetic microrobot (b) Diagram of magnetic alignments and induced magnetic torque.

$$\vec{T}_m = V_m \vec{M} \times \vec{B} \tag{1}$$

Eq. 1 describes the general working principle of this torque, where V_m is the magnetic volume of the robot, $\vec{M}$ is the magnetization of the robot, and $\vec{B}$ is the external magnetic field strength. Under a time-varying rotating magnetic field, the torque causes the microrobot to undergo a forward tumbling motion.

Fig. 2 depicts the resulting motion of the microrobot over a flat surface with no-slip conditions. While a cylindrical design would result in a more uniform rolling motion, standard MEMS fabrication techniques limit the thickness of the polymer block. A thin, rolling cylinder tends to tip over on rough surfaces, where small disturbances upset the stability of the cylinder, making a tumbling block better suited for biomedical applications.

C. Fabrication Method

Fig. 3 summarizes the entire fabrication and magnetization procedure for the new microrobot design. First, SU-8 50 photoresist is doped with NdFeB particles (Magnequench MQFT 5 μm, Neo Magnequench) at a concentration of 15g/50mL. The doped SU-8 is then spin-coated at 1000 rpm for 60 s and undergoes a two-step soft-baking process of 10 min at 65°C and 30 min at 95°C. These steps are used to obtain a thick layer of SU-8, approximately 120 μm, and to evaporate the excess solvent. Next, the wafer is exposed to UV light in a mask aligner (Suss MA6 Mask Aligner, SUSS MicroTec AG) using a mask corresponding to the geometry of the microrobot for 70 s. A post-exposure bake of 1 min at 65°C and 10 min at 95°C is then performed to selectively cross-link the exposed areas of the film. Lastly, the non-polymerized SU-8 is removed with SU-8 developer (Microchem Inc.) in a bath for 10 min and then the wafer is cured in an oven at 160°C. Unlike previous versions of this microrobot [22], the fabrication process has been reduced

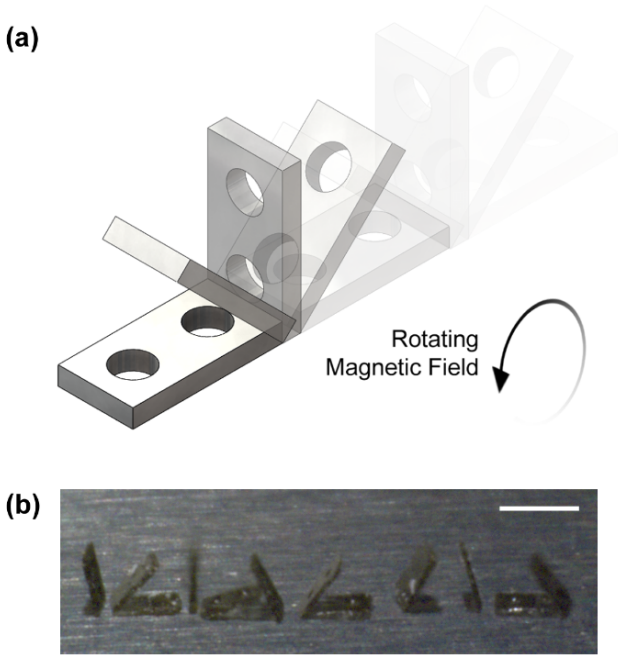

Fig. 2. (a) Depiction of microrobot tumbling movement (b) Motion lapse of tumbling movement over aluminum surface. Scale bar is 1 mm.

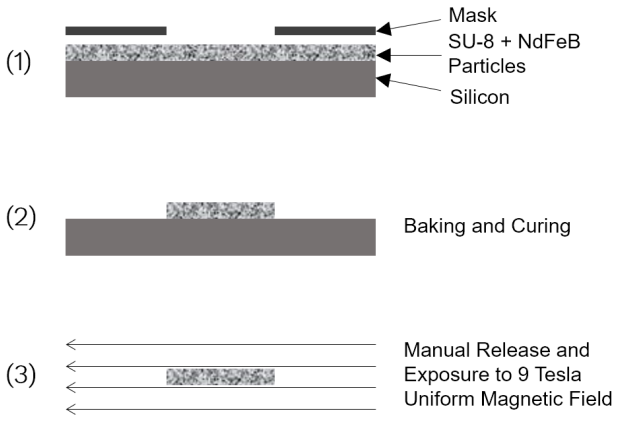

Fig. 3. Photolithography and magnetization process for the fabrication of the microscale magnetic robot.

to a simple, one-step photolithography process. In this case, the middle portion of the robot that required an additional photolithography step is not necessary to store a payload.

Once the microrobot fabrication is complete, the robot is manually removed from the wafer using tweezers and a utility knife. The magnetic particles are then aligned along the same direction using a strong external magnetic field, greatly improving the magnetic polarity of the microrobot and their responsiveness under lower magnetic field strengths. The robot is secured in the desired orientation during the magnetization process on a quartz sample holder using Kapton tape (Dupont). The external field is generated using the PPMS Dynacool machine (Quantum Design), which is capable of applying uniform magnetic fields of up to 9 T.

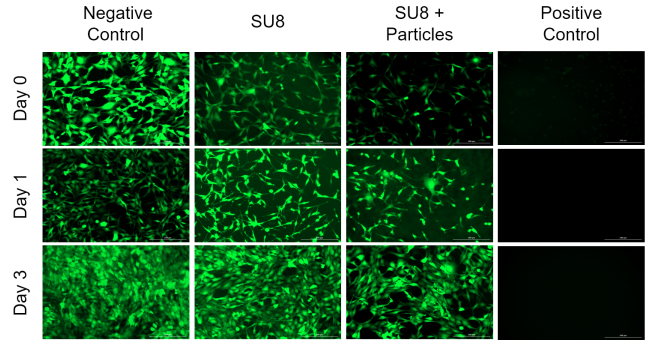

Fig. 4. Fluorescent images taken of cell proliferation for four different test cases. Green fluorescent cells indicate living cells that have adhered to the well plate and are viable.

III. BIOMEDICAL APPLICATIONS TESTING

A. Cytotoxicity Tests

To assess the short-term cytotoxicity of the doped SU-8 used to fabricate the microrobots, the cell viability of NIH3T3 murine fibroblasts in direct contact with the materials was studied over the course of 3 days, with day 0 measurements taken 12 hours after initial seeding. The NIH3T3 fibroblasts were seeded on surfaces of both SU-8 and SU-8 with NdFeB particles, and were compared to negative and positive controls consisting of tissue culture polystyrene and cells cultured in 70% ethanol, respectively, to elicit a cytotoxic response. Proliferation was examined using fluorescence microscopy (BioTek Cytation5 Cell Imaging Multi-Mode Reader). Fig. 4 indicates cell proliferation on doped SU-8 and the cells do not exhibit signs of short-term toxicity. As expected, the negative control experienced cell proliferation while the positive control had no living cells after 3 days.

B. Payload Diffusion Tests

The diffusion characteristics of a fluorescent payload coating the microrobot were quantified to explore targeted drug delivery applications. The microrobots were coated with a PLGA solution consisting of N-methyl pyrrilidone (NMP), poly(lactic-co-glycolic acid) (PLGA), and fluorescein. The coated microrobots were then placed into 1 mL of phosphate buffered saline (PBS) in a 2 mL serum vial. These were kept at 37°C on a shaker at 100 rpm. Samples were taken from the bath-side solution at 0.25, 0.5, 1, 2, 4, 6, 24, 48, 96, and 120 hours after initial coating. The bath solution was replaced with fresh PBS at all sampling time points to maintain conditions. After 168 hours (7 days), the coated microrobots were dissolved in NaOH to determine any residual drug mass. The fluorescence of each sample was quantified afterwards using a SpectraMax M5 microplate reader. The samples were read at an excitation wavelength of 485 nm and emission wavelength of 525 nm. The results shown in Fig. 5 were obtained by comparing experimental measurements against a standard curve of absorbance values, which itself was generated by making solutions with known fluorescence concentrations. The experiment was ran in triplicate to reduce

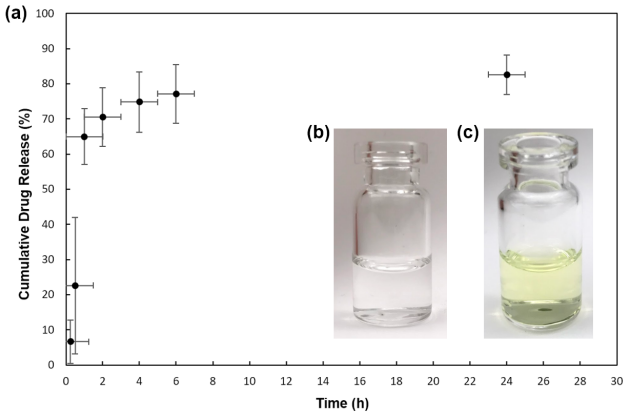

Fig. 5. (a) Cumulative mass data of diffusion study (for the first 24 hours) (b) Microrobot initially placed in glass vial (c) Microrobot in vial and PBS 24 hours later. Green solution is fluorescein released from PLGA coating.

the possibility of experimental bias or random error. It can be observed that most of the payload diffuses within the first two hours of resting in the PBS bath. This should be a sufficiently long time for the microrobot to travel from desired point of entry in the body to a nearby target location.

C. Murine Locomotion Tests

Real-time videos of the microrobots were acquired using a high-frequency ultrasound system (Vevo3100, FUJIFILM VisualSonics). A linear array ultrasound probe (MX700) with a frequency range of 30 to 70 MHz and a central frequency of 50 MHz was used to image euthanized C57BL/6 female apolipoprotein E (*apoE*$^{-/-}$) knockout mice at 12 weeks of age. A cylindrical NdFeB permanent magnet (1" diameter x 0.875" thick, Cyl1875, SuperMagnetMan) was rotated at a frequency of 1 Hz underneath the animal, applying torque on a microrobot inserted inside the animal's colon. Using the model presented in [23], the magnetic field strength of the magnet at the location of the microrobot is approximately 21.4 mT. The direction of the robot's movement can be controlled by reversing the rotation of the magnet or changing its axis of rotation. Fig. 6 illustrates the imaging setup with the probe placed above the specimen and the magnet placed below it. Microrobot movement was tested for *in vitro*, *in situ* dissected, and *in situ* intact conditions. Average velocities, $\bar{v}$, were calculated for each condition using Eq. 2,

$$\bar{v} = \frac{\Delta x}{\Delta t} = \frac{x_f - x_0}{t_f - t_0} \tag{2}$$

where Δx represents the change in position, from the final position, x_f, to the initial position, x_0, and Δt represents the change in time, from the final timepoint, t_f, to the initial timepoint, t_0, as shown in Table 1 [24].

1) in vitro Tests: The *in vitro* tests consisted of a 1% agarose gel block with a 3.175 mm in diameter hole traveling through the the block. A glass dish filled with water contained the agarose gel, and the robot was subsequently placed inside the hole. The magnet was rotated as B-mode images were acquired. Fig. 7 shows the microrobot traveling through the water-filled agarose tube with ease at 2.2 mm/s.

TABLE I
MICROROBOT VELOCITIES IN DIFFERENT TEST CONDITIONS

Test Condition	Water *in vitro*	Saline *in situ* dissected	1% Tylose *in situ* intact
Trial 1 (mm/s)	2.23	1.96	0.19
Trial 2 (mm/s)	2.21	1.89	0.19
Trial 3 (mm/s)	2.23	1.87	0.25
Average Velocity (mm/s)	2.23	1.91	0.21
Standard Deviation (mm/s)	0.01	0.05	0.04

2) in situ Dissected Tests: For the *in situ* dissected tests, tissue anterior to the colon was removed and the robot was placed inside the colon of the mouse through the anus. The *in situ* tests involved filling the colon retrograde with solution and acquiring B-mode long-axis images of the mid and distal regions [25]. Saline was used as the solution for the dissected tests and the colon was subsequently sutured on both ends in order to ensure the liquid remained within the colon. Fig. 8 shows the microrobot traveling through the colon at roughly 1.9 mm/s.

3) in situ Intact Tests: For the *in situ* intact tests, the tissue anterior to the colon was left in place while the robot was again inserted into the anus of the mouse. The colon was filled with a 1% Tylose solution [26] and the robot moved through the colon via the rotating magnet. This solution was much more viscous than water or saline, which allowed for the solution to support the shape of the colon without the need of other constructs such as sutures. Solutions that are even more viscous than 1% Tylose, such as standard ultrasound gel, posed problems for microrobot movement. Within these substances, the robot has difficulty translating

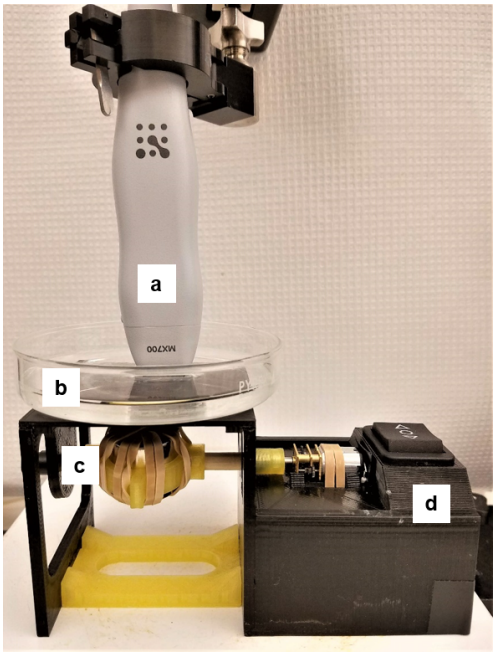

Fig. 6. The imaging acquisition setup with a (a) probe, (b) specimen platform, (c) magnet, and (d) magnet motor.

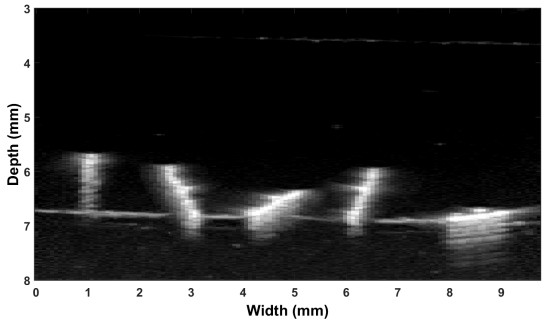

Fig. 7. *in vitro* Tests: Ultrasound B-mode motion lapse of microrobot moving through water in a 1% agarose tube over a 4 second time period.

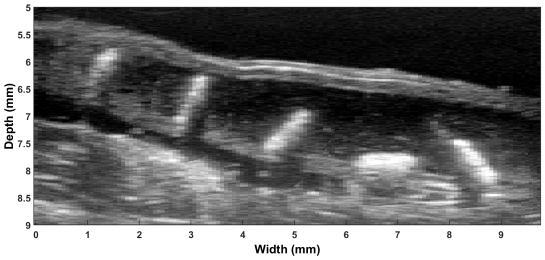

Fig. 8. *in situ* Dissected Tests: Ultrasound B-mode motion lapse of microrobot traveling within the sutured off colon filled with saline over a 3 second time period.

along the length of the tissue. Fig. 9 displays the robot moving through the colon at roughly 0.2 mm/s.

As displayed in Table 1, the velocities varied greatly among the different conditions. The aqueous *in vitro* tests had the largest velocity, the *in situ* dissected experiments in saline had a slightly smaller velocity, while the *in situ* intact tests in 1% Tylose demonstrated the smallest velocity. This is likely due to the differences in viscosity of the solutions as well as the terrain of the test environment. In other words, the robot was slowed, in part, due to viscous drag. The 1% Tylose solution is much more viscous than the aqueous environments used in the in the other tests. While the viscosity of water is about 0.89 mPa.s, the 1% Tylose solution is more viscous at a value of 4500 mPa.s [27]. The environment of each test also needs to be accounted for with differences in the heterogeneity of the terrain and the coefficient of friction, thereby creating a difference in the ability of the robot to grip the surface, travel across the surface, as well as travel through the solution. Looking at the standard deviations, they were greater in the *in situ* tests than the *in vitro* tests. This makes sense as the *in vitro* tests provide a homogeneous surface for the robot, while the *in situ* tests had a varying surface down the length of the colon. In summary, the microrobot maintained its ability to move due to a rotating magnet through a wide variety of *in vitro* and *in situ* conditions.

IV. CONCLUSIONS

This paper presented a magnetic tumbling microrobot capable of locomotion in multiple biological environments.

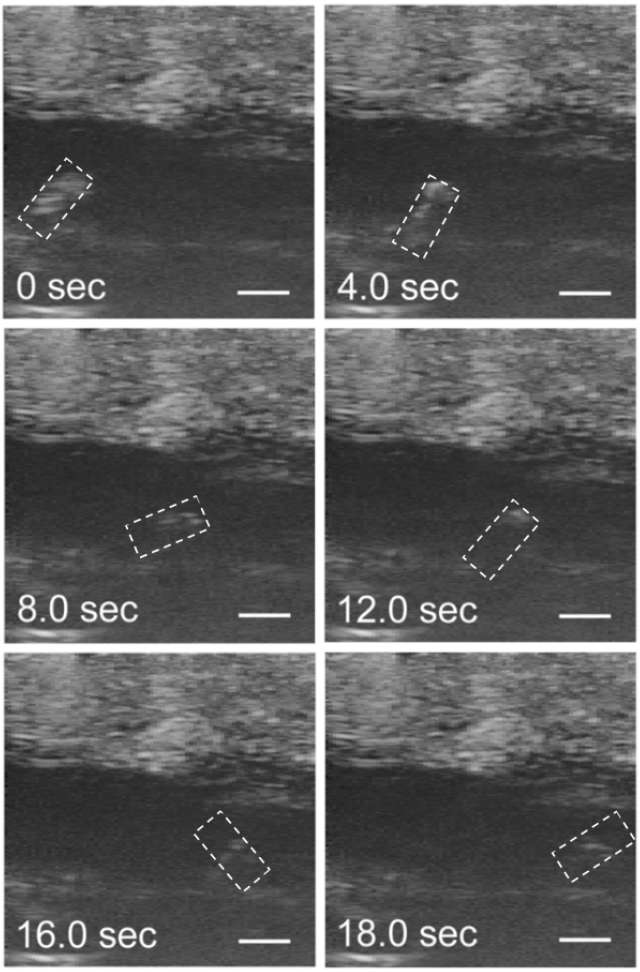

Fig. 9. *in situ* Intact Tests: Ultrasound B-mode image sequence of microrobot traveling through a 1% Tylose solution in the colon over an 18 second time period. Scale bar is 1 mm.

Its ability to traverse through an intact *in situ* murine colon demonstrates potential for similar capabilities inside human colons that are substantially larger. Ultrasound imaging allowed for real-time tracking of the robot's position and orientation even when it was optically occluded. The microrobot was able to retain a fluorescent imaging payload and gradually release it over a 10 hour period. The microrobot was also found to be biocompatible with murine fibroblasts after a short-term cytoxicity test. The biomedical applications for this robot will vary depending on its outer coating and surface treatment. The ability to travel non-invasively to a desired location within the colon will be useful for targeted drug delivery, tissue biopsies, and detoxification applications within the surrounding area. The microrobot may prove to be valuable in treating disorders in other parts of the body as well, given its ability to traverse through difficult environments while being tracked in real-time.

Future work will consider non-uniform magnetic alignment to allow for multi-modal locomotion, closed-loop control of the robot with computer vision algorithms, and *in vivo* testing of targeted drug delivery in live mice.

ACKNOWLEDGMENT

The authors acknowledge the facility access at Birck Nanotechnology Center (Purdue University).

REFERENCES

[1] M. Luo, Y. Feng, T. Wang, and J. Guan, "Micro-/Nanorobots at Work in Active Drug Delivery," *Advanced Functional Materials*, vol. 28, no. 25, pp. 1–23, 2018.

[2] Y. Alapan, O. Yasa, M. Sitti, P. Erkoc, I. C. Yasa, and H. Ceylan, "Mobile Microrobots for Active Therapeutic Delivery," *Advanced Therapeutics*, vol. 2, no. 1, p. 1800064, 2018.

[3] E. M. Purcell, "Life at low Reynolds number," *American Journal of Physics*, vol. 45, no. 1, pp. 3–11, 1977. [Online]. Available: http://aapt.scitation.org/doi/10.1119/1.10903

[4] M. Sitti, *Mobile microrobotics*, ser. Intelligent robotics and autonomous agents. The MIT Press, 2017.

[5] Y. Zhang, K. Yuan, and L. Zhang, "Micro/Nanomachines: from Functionalization to Sensing and Removal," *Advanced Materials Technologies*, vol. 1800636, pp. 1–22, 2019.

[6] W. Gao, R. Dong, S. Thamphiwatana, J. Li, W. Gao, L. Zhang, and J. Wang, "Artificial micromotors in the mouse's stomach: A step toward in vivo use of synthetic motors," *ACS Nano*, vol. 9, no. 1, pp. 117–123, 2015.

[7] J. Li, B. E.-f. D. Ávila, W. Gao, L. Zhang, J. Wang, B. Esteban-Fernández De Ávila, W. Gao, L. Zhang, and J. Wang, "Micro / nanorobots for biomedicine : Delivery , surgery , sensing , and detoxification," *Sci. Robot*, vol. 2, no. 1, pp. 1–10, 2017.

[8] D. Kagan, M. J. Benchimol, J. C. Claussen, E. Chuluun-Erdene, S. Esener, and J. Wang, "Acoustic droplet vaporization and propulsion of perfluorocarbon-loaded microbullets for targeted tissue penetration and deformation," *Angewandte Chemie - International Edition*, vol. 51, no. 30, pp. 7519–7522, 2012.

[9] E. Diller, "Micro-Scale Mobile Robotics," *Foundations and Trends in Robotics*, vol. 2, no. 3, pp. 143–259, 2011. [Online]. Available: http://www.nowpublishers.com/articles/foundations-and-trends-in-robotics/ROB-023

[10] I. Ordás, L. Eckmann, M. Talamini, D. C. Baumgart, and W. J. Sandborn, "Ulcerative colitis," *The Lancet*, vol. 380, no. 9853, pp. 1606–1619, 2012.

[11] M. J. Denters, M. Schreuder, A. C. Depla, R. C. Mallant-Hent, M. C. A. v. Kouwen, M. Deutekom, P. M. Bossuyt, P. Fockens, and E. d. Dekker, "Patients' perception of colonoscopy: patients with inflammatory bowel disease and irritable bowel syndrome experience the largest burden," *European Journal of Gastroenterology & Hepatology*, vol. 25, pp. 964–972, 2013.

[12] S. Menees, P. Higgins, S. Korsnes, and G. Elta, "Does colonoscopy cause increased ulcerative colitis symptoms?" *Inflammatory Bowel Diseases*, vol. 13, no. 1, pp. 12–18, 2007.

[13] T. Ogawa, Y. Ohda, K. Nagase, T. Kono, K. Tozawa, T. Tomita, M. Iimuro, N. Hida, T. Oshima, H. Fukui, K. Hori, J. Watari, S. Nakamura, and H. Miwa, "Evaluation of discomfort during colonoscopy with conventional and ultrathin colonoscopes in ulcerative colitis patients," *Digestive Endoscopy*, vol. 27, no. 1, pp. 99–105, 2015.

[14] F. Parente, M. Molteni, B. Marino, A. Colli, S. Ardizzone, S. Greco, G. Sampietro, D. Foschi, and S. Gallus, "Are colonoscopy and bowel ultrasound useful for assessing response to short-term therapy and predicting disease outcome of moderate-to-severe forms of ulcerative colitis: A prospective study," *American Journal of Gastroenterology*, vol. 105, no. 5, pp. 1150–1157, 2010. [Online]. Available: http://dx.doi.org/10.1038/ajg.2009.672

[15] S. Takashima, J. Kato, S. Hiraoka, A. Nakarai, D. Takei, T. Inokuchi, Y. Sugihara, M. Takahara, K. Harada, H. Okada, T. Tanaka, and K. Yamamoto, "Evaluation of mucosal healing in ulcerative colitis by fecal calprotectin vs. fecal immunochemical test," *American Journal of Gastroenterology*, vol. 110, no. 6, pp. 873–880, 2015. [Online]. Available: http://dx.doi.org/10.1038/ajg.2015.66

[16] M. Medina-Sánchez, L. Schwarz, A. K. Meyer, F. Hebenstreit, and O. G. Schmidt, "Cellular Cargo Delivery: Toward Assisted Fertilization by Sperm-Carrying Micromotors," *Nano Letters*, vol. 16, no. 1, pp. 555–561, 2016.

[17] R. Pieters, H. W. Tung, S. Charreyron, D. F. Sargent, and B. J. Nelson, "RodBot: A rolling microrobot for micromanipulation," *Proceedings - IEEE International Conference on Robotics and Automation*, vol. 2015-June, no. June, pp. 4042–4047, 2015.

[18] W. Hu, G. Z. Lum, M. Mastrangeli, and M. Sitti, "Small-scale soft-bodied robot with multimodal locomotion," *Nature*, vol. 554, no. 7690, pp. 81–85, 2018. [Online]. Available: http://dx.doi.org/10.1038/nature25443

[19] S. Floyd, C. Pawashe, and M. Sitti, "An untethered magnetically actuated micro-robot capable of motion on arbitrary surfaces BT - 2008 IEEE International Conference on Robotics and Automation, ICRA 2008, May 19, 2008 - May 23, 2008," pp. 419–424, 2008. [Online]. Available: http://dx.doi.org/10.1109/ROBOT.2008.4543243

[20] H. W. Tung, M. Maffioli, D. R. Frutiger, K. M. Sivaraman, S. Pané, and B. J. Nelson, "Polymer-based wireless resonant magnetic microrobots," *IEEE Transactions on Robotics*, vol. 30, no. 1, pp. 26–32, 2014.

[21] W. Jing, N. Pagano, and D. J. Cappelleri, "A tumbling magnetic microrobot with flexible operating modes," *Proceedings - IEEE International Conference on Robotics and Automation*, pp. 5514–5519, 2013.

[22] C. Bi, M. Guix, B. V. Johnson, W. Jing, and D. J. Cappelleri, "Design of microscale magnetic tumbling robots for locomotion in multiple environments and complex terrains," *Micromachines*, vol. 9, no. 2, pp. 1–17, 2018.

[23] J. M. Camacho and V. Sosa, "Alternative method to calculate the magnetic field of permanent magnets with azimuthal symmetry," *Revista mexicana de física E*, vol. 59, pp. 8–17, 2013.

[24] D. Halliday, R. Resnick, and J. Walker, *Fundamentals of Physics*, 9th ed., G. Osnato, S. Johnson, A. Rentrop, E. Swain, H. Newman, and T. Kulesa, Eds. Hoboken: John Wiley & Sons, Inc., 2011.

[25] J. L. Freeling and K. Rezvani, "Assessment of murine colorectal cancer by micro-ultrasound using three dimensional reconstruction and non-linear contrast imaging," *Molecular Therapy - Methods and Clinical Development*, vol. 3, no. July, p. 16070, 2016.

[26] T. Heinar, "Medical gel," U.S. Patent 0 116 331, May 9, 2013.

[27] Shin-Etsu, "Tylose for Personal Care," SE Tylose GmbH & Co., 2015.